33rd Annual International Conference of the IEEE EMBS
Boston, Massachusetts USA, August 30 - September 3, 2011

Retinal Vessel Extraction by Combining Radial Symmetry Transform and Iterated Graph Cuts

Dehui Xiang, Jie Tian *, *Fellow, IEEE*, Kexin Deng, Xing Zhang, Fei Yang and Xiaonan Wan

***Abstract*— In this paper, we propose a new method for the extraction of blood vessels in retinal images. This approach starts with a Hessian-based multiscale filtering method to enhance blood vessels in gray retinal images. Subsequently, a new radial symmetry transformation, which is based on line kernels, is proposed to improve the detection of vessel structures and restrain the response of nonvessel structures. Finally, an iterated segmentation algorithm is used to extract retinal vessels. The proposed approach has been tested on the two publicly available databases, DRIVE and STARE. The experimental results show the feasibility of the proposed method.**

I. INTRODUCTION

The extraction of blood vessels is an especially challenging problem in fundus imaging. This is due to the complexity and variability of their anatomic structures. As one of the main structures in retinal images, retinal vessel trees are usually distorted and deformed by various retinopathies such as glaucoma, artery occlusion, microaneurysms and choroidal neovascularization [1], [2], [3], [4]. Various non-ophthalmic diseases such as diabetes, hypertension, and cardiovascular disease may lead to blood vessels pathological changes [5] and retinal diseases [6].

Tremendous amount of dedicated researches have been done to develop better retinal vessel extraction algorithms in recent years. Some approaches were presented based on a combination of multiscale filtering and classification [7], [8]. Many other approaches have been introduced, centerline tracking [5], hermite model [9], and multiconcavity modeling [6] etc. In this paper, we propose a new method for the extraction of blood vessels in retinal images. In the preprocessing step, a Hessian-based multiscale filtering method is used to enhance blood vessels in gray retinal images, and to obtain the direction and radii of blood vessels. Subsequently, a new radial symmetry transformation, which is based on line kernels, is introduced to remove the response of nonvessel structures. Finally, an iterated segmentation algorithm is used to extract the retinal vessels.

This paper is supported by the National Basic Research Program of China (973 Program) under Grant 2011CB707700, the National Natural Science Foundation of China under Grant No. 81071218, 60910006, 30873462, the Knowledge Innovation Project of the Chinese Academy of Sciences under Grant No.KSCX2-YW-R-262.

D. Xiang, J. Tian, K. Deng, X. Zhang, F. Yang and X. Wan are with Intelligent Medical Research Center, Institute of Automation, Chinese Academy of Sciences, Beijing, 100190, China. tian@ieee.org

II. METHOD

A. Preprocessing

In order to enhance tubular structures of various widths, it is necessary to consider a multiscale filtering method. In this framework, the images are convolved with a set of 2D Gaussian derivative filters at multiple scales and a few response functions are formulated according to the eigenvalues of the Hessian matrix to detect interested structures (see Fig.4(b)). Let $\lambda_{s,1}$, $\lambda_{s,2}$ are the eigenvalues of Hessian matrix at a scale s, vascular structures can be enhanced by the multiscale line response function [10],

$$V = \max_{s_{\min} \le s \le s_{\max}} v_s \tag{1}$$

where,

$$v_s = \begin{cases} \frac{|\lambda_{1,s}|+|\lambda_{2,s}|}{2} \mathrm{e}^{\left(-\left|\frac{|\lambda_{1,s}|}{\sqrt{\lambda_{1,s}^2+\lambda_{2,s}^2}}-c\right|\right)}, & \lambda_{1,s},\lambda_{2,s}<0 \\ 0, & otherwise \end{cases};$$

c is a constant. We can obtain the scales of vascular structures in the enhanced images. The contours of structures with the scales are determined by Canny edge detector.

B. Radial Symmetry Transform

Though the multiscale filters enhanced tubular structures, they produce boundary effects around the pathological changes, the optic disc (shown in Fig.2 (a)-(b)). These spurious responses are sometimes stronger than the responses to narrow vessels and low contrast vessels (shown in Fig.2 (c)-(d)). A further process is a requisite for the removal of nonvessel responses [7]. We now introduce a fast radial symmetry transform [11] to suppress those artifacts.

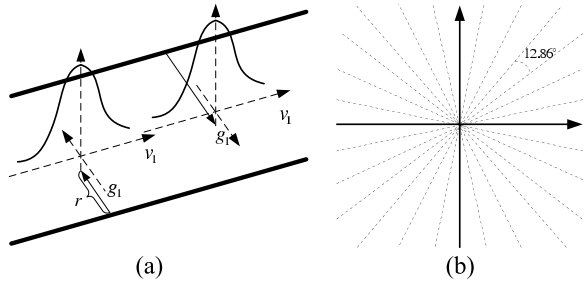

Fig. 1. The radial symmetry transform. (a) The contribution S to vessels from their neighboring pixels along the direction of the vessels and the the gradient of edges. (b) Fourteen line kernels.

The basic idea is illustrated in Fig.1(a). The radial symmetry transform is achieved by computing the contribution S for each pixel from their neighboring pixels along the direction

of the gradients. A oriented line kernel L_n with its size $n \times n$ is then applied along the tangential direction in order to disperse the influence of the effected pixels and produce smoothed vessels. We have noticed that the boundary effects unilaterally proliferate. For bilateral structures like vessels the symmetry contribution values from edges are at lest as two times as that from unilateral structures.

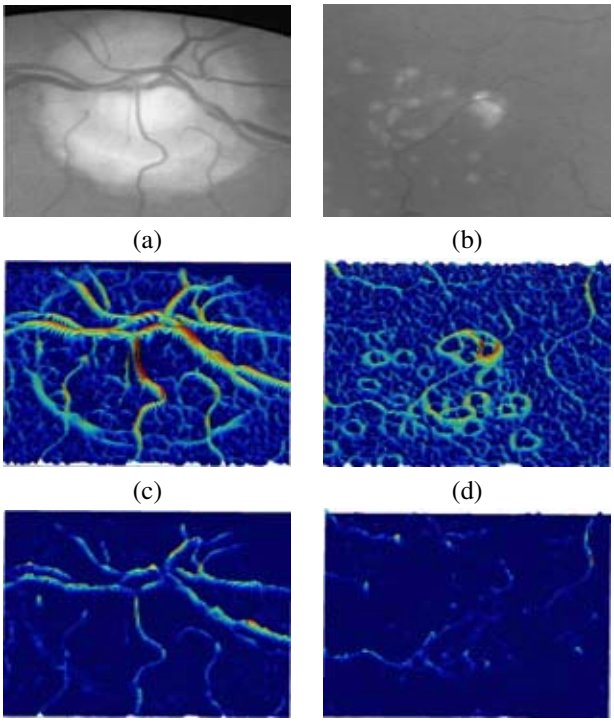

Fig. 2. Some results after radial symmetry transform. (a) Optic disk; (b) Pathological changes; (c)-(d) The multiscale filtered results; (e)-(f) The results after radial symmetry transform.

After compute the gradient field $\overrightarrow{G}(p)$ for each pixel $p(i,j)$ on the contours, the gradient vectors are normalized as $\overrightarrow{g}(p) = \overrightarrow{G}(p) / ||\overrightarrow{G}(p)||$. Then, the coordinates of the affected pixels are given by

$$p_r(p) = p + round\left(r \cdot \overrightarrow{g}(p)\right) \tag{2}$$

where r denotes the distance between a pixel on the edge and the corresponding affected pixel, $r = 0, \Delta r, \cdots, 2R$; R is the radius of a vessel obtained from the proposed multiscale filters. The orientation projection image O is updated by

$$O(p_r(p)) \leftarrow O(p_r(p)) + 1 \tag{3}$$

In [11], the magnitude projection image is incremented by $||\overrightarrow{g}(p)||$. In order to preserve tubular structures, the radial symmetry contribution however is determined by the local value of the affected pixel,

$$F = V \cdot \left(\frac{O}{k}\right)^{\gamma} \tag{4}$$

where, k is a normalizing factor; γ is a radial strictness parameter.

To obtain smoothed vessels, the radial symmetry contribution F must be dispersed and convolved with an oriented line kernel L_n. Before applying the convolution with a given line kernel, all pixels, of which the angles are between d and $d + \Delta d$, are chosen out as a new image F_d from the image F. The final radial symmetry transform is defined as

$$S = \sum_{d=\Delta d, 2\Delta d, \cdots, 180^\circ} F_d * L_n(d) \tag{5}$$

We choose the eigenvector of $\lambda_{s,1}$ as the orientation of L_n, $n = 7$. Fourteen line kernels are generated with about a $\Delta d = 12.86^\circ$ increment and then stored in a code book (see Fig.1(b)). As shown in Fig.2(e)-(f), the responses from the boundaries of optic disk and the pathological changes are evidently filtered out and blood vessels are still left.

C. The Iterated Graph Cuts Algorithm

Having enhanced all potential tubular structures and suppressed noise in the background, the final step is to accurately segment vessels from the two previous processing results. The image segmentation can be converted into a problem that a label is properly assigned to each pixel. Such pixel-labeling problems can be often formulated using the energy function,

$$E(\mathcal{L}) = E_d(\mathcal{L}) + \kappa E_s(\mathcal{L}) \tag{6}$$

where, $\mathcal{L}$ is a labeling set; $E_d(\mathcal{L}) = \sum_{p \in \mathcal{P}} U_p(l_p)$ is the data priori energy in the whole pixel set $\mathcal{P}$ of the observed data, which measures the cost of giving a label $l_p \in \mathcal{L}$ to an given pixel p according to priori information; $E_s(\mathcal{L}) = \sum_{\mathcal{N} \subset \mathcal{P}} \sum_{q \in \mathcal{N}} V_{pq}(l_p, l_q)$ is the clique potential energy, which measures the smoothness of a neighboring pixel system $\mathcal{N}$, $l_q \in \mathcal{L}$; κ is a weighted parameter.

Traditional graph cuts methods are easily trapped in local minima though extremely fast in convergence, because most vessels are slim and spiky in a retinal image. To optimize the energy function (6) and provide a better separation of vessels from retinal images, centerline is used as shape prior to guide the extraction process; meanwhile, radial symmetry is also utilized to constrain the graph cuts algorithm. A thresholding method is applied to the results S obtained from radial symmetry transform such that pixels $S \geq t_h$ are picked out, and then thin the thresholded image. We discard segments with less than 20 pixels to further remove non-vessel structures.

In our framework, a graph $\mathcal{G} = \langle \mathcal{V}, \mathcal{E} \rangle$ is created with nodes corresponding to pixels $p \in \mathcal{P}$ of a retinal image, where $\mathcal{V}$ is the set of all nodes and $\mathcal{E}$ is the set of all links connecting neighboring nodes. The neighboring pixel system $\mathcal{N}$ is constructed with eight neighboring pixels. The *terminal* nodes are still defined as: source $\mathcal{S}$ and sink $\mathcal{T}$. The *unlabeled* nodes are defined with another thresholding value as another two types: *candidate foreground* $\mathcal{F}_c$ and *candidate background* $\mathcal{B}_c$. Initially, the pixels on the centerline are considered as the nodes in *definite foreground* $\mathcal{F}_d$, and the pixels $S \leq t_l$ are classified as the nodes in

definite background $\mathcal{B}_d$. That is, $\mathcal{L} = \{f_d, b_d, f_c, b_c\}$ and $\mathcal{V} = \{\mathcal{S}, \mathcal{T}\} \cup \{\mathcal{F}_d, \mathcal{B}_d\} \cup \{\mathcal{F}_c, \mathcal{B}_c\}$.

We compute the minimum distance $d_f(p)$ and $d_b(p)$ between a pixel $p \in \{\mathcal{F}_c, \mathcal{B}_c\}$ to $\mathcal{S}$ and $\mathcal{T}$ [12]. The cost of *t-links* can be computed via,

$$\begin{cases} U_{\mathcal{S}}(p) = \infty, & U_{\mathcal{T}}(p) = 0, & p \in \mathcal{F}_d; \\ U_{\mathcal{S}}(p) = 0, & U_{\mathcal{T}}(p) = \infty, & p \in \mathcal{B}_d; \\ U_{\mathcal{S}}(p) = \frac{\omega_1 S(p)}{D_{\mathcal{F}}(p)}, & U_{\mathcal{T}}(p) = \frac{\omega_2 S(p)}{D_{\mathcal{F}}(p)}, & p \in \mathcal{F}_c; \\ U_{\mathcal{S}}(p) = \frac{\omega_2 S(p)}{D_{\mathcal{F}}(p)}, & U_{\mathcal{T}}(p) = \frac{\omega_1 S(p)}{D_{\mathcal{B}}(p)}, & p \in \mathcal{B}_c; \end{cases} \tag{7}$$

where, $D_{\mathcal{F}}(p) = \frac{d_f(p)}{d_f(p)+d_b(p)}$, $D_{\mathcal{B}}(p) = \frac{d_b(p)}{d_f(p)+d_b(p)}$, and $\omega_1 > 1 > \omega_2 > 0$. The nodes in $\mathcal{F}_d$ and $\mathcal{B}_d$ are definitely labeled as f_d and b_d respectively, and will not be relabeled any more. We encourage *candidate foreground* pixels to be labeled as foreground seeds while discourage them to be classified as background pixels, vice versa.

The weight of *n-link* describes the labeling coherence of a pixel with its neighbors. We utilize radial symmetry information again to improve the segmentation. Then, the cost of *n-links* can be defined as,

$$V_{pq}(l_p, l_q) = \frac{1}{|V(p) - V(q)| \cdot |S(p) - S(q)|} \tag{8}$$

This equation allows an effective simultaneous parameter estimation and optimization, which is less affected by the possibly negative role of pathological changes, optic disc, etc.

The proposed graph cuts method works iteratively, with each iteration an optimization process for finding a local minimum of the objective energy function (6). The process begins with a coarse labeling configuration with totally four classes and tries to reduce to two classes. Examining each pixel in $\mathcal{F}_c$ and $\mathcal{B}_c$, its local energy is defined as

$$e_p(l_p) = u_p(l_p) + \kappa e_{\mathcal{N}}(l_p) \tag{9}$$

where,

$$u_p(l_p) = \begin{cases} D_{\mathcal{F}}(p), & l_p = f_c; \\ D_{\mathcal{B}}(p), & l_p = b_c; \end{cases} \tag{10}$$

$e_{\mathcal{N}}(l_p) = \sum_{q \in \mathcal{N}} v_{pq}(l_p, l_q)$, and $v_{pq}(l_p, l_q)$ is given in the following table,

	$l_q = b_d$	$l_q = b_c$	$l_q = f_c$	$l_q = f_d$
$l_p = b_c$	-1	$-\zeta$	ζ	1
$l_p = f_c$	1	ζ	$-\zeta$	-1

$0 \le \zeta \le 1$, the local energy is divided into three intervals. If e_p achieves a level, a label change is justified. The relabeling process can be formulated as,

$$l_p' = \begin{cases} b_c, & \eta_{f_c,1} \le e_p(l_p = f_c); \\ f_c, & \eta_{f_c,2} \le e_p(l_p = f_c) < \eta_{f_c,1}; \quad or, \\ f_d, & e_p(l_p = f_c) < \eta_{f_c,2}. \end{cases}$$

$$l_p' = \begin{cases} f_c, & \eta_{b_c,1} \le e_p(l_p = b_c); \\ b_c, & \eta_{b_c,2} \le e_p(l_p = b_c) < \eta_{b_c,1}; \\ b_d, & e_p(l_p = b_c) < \eta_{b_c,2}. \end{cases} \tag{11}$$

where, $\eta_{f_c,1}$ and $\eta_{f_c,2}$ are two local energy level constants for the pixels labeled as *candidate foreground*; $\eta_{b_c,1}$ and $\eta_{b_c,2}$ are two local energy level constants for the pixels labeled as *candidate background*.

After the label growing and changing process is completed, the graph cuts algorithm is repeatedly applied [13] till it achieves a maximum number of iterations ($n_{iter} = 8$). The graph is re-parameterize such that it maintains the flow properties after updating the weights of edges by the formula (7) and (8) according to the current labeling configuration. Label change and re-parametrization are two basic procedures involved in the dynamic graph cuts algorithm. The label change procedure works in a greedy way to find a proper label for each pixel in the retinal images obtained by a local energy criterion from the previous iteration.

III. EXPERIMENTS AND RESULTS

A. Images and Evaluation

We have tested our method on the two publicly available databases, STARE [14] (20 images) and DRIVE [15] (20 images). Three measures sensitivity (SE), specificity (SP) and accuracy (AC) are used to evaluate the performance of our method in the image field of view (FOV). The sensitivity is defined as the ratio of the number of correctly classified vessel pixels by the number of the vessel pixels in ground truth. The specificity is computed by the ratio of the number of correctly classified non-vessel pixels by the number of the non-vessel pixels in ground truth. The accuracy is calculated as the number of correctly classified vessel pixels plus the number of correctly classified non-vessel pixels divided by the number of all pixels in FOV.

B. Results

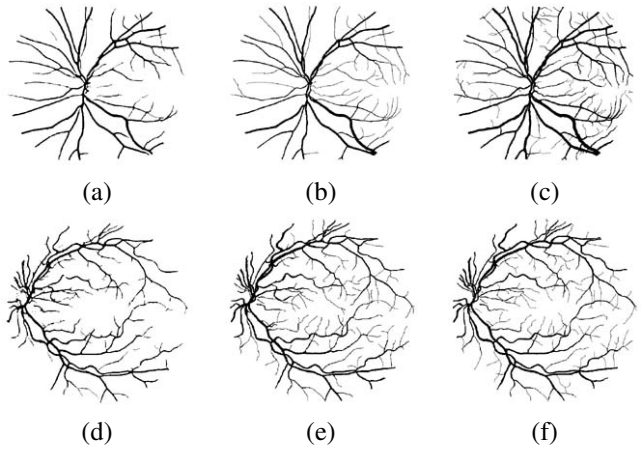

Fig. 3. Two examples of vessel extraction for normal images. (a) The final segmentation by the proposed method (STARE); (b)-(c) Manual segmentations; (d) The final segmentation by the proposed method (DRIVE); (e)-(f) Manual segmentations.

Fig.3 shows two normal cases of vessel extraction by the proposed method. The first results are obtained from the STARE database shown in Fig.3(a)-(c), and the second results are obtained from the DRIVE database shown in Fig.3(d)-(f). The first column images are the final segmentation results. The other two columns are the manual

segmentation results. Fig.2 and Fig.4 show an example of vessel extraction for a pathological image.

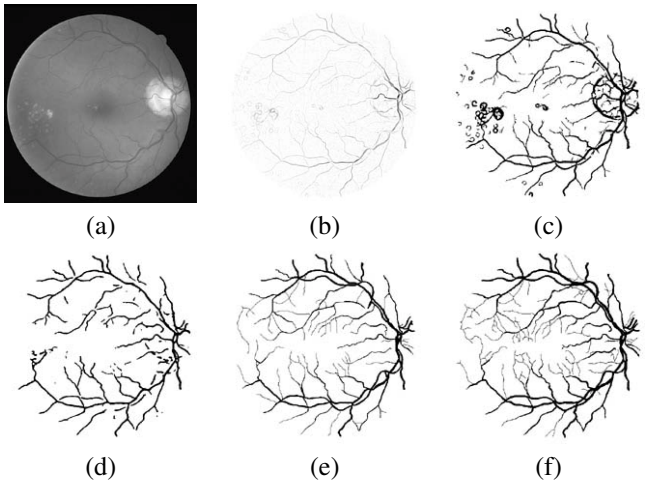

Fig. 4. An example of vessel extraction for a pathological image. (a) The original gray image; (b) The multiscale filtered result; (c) The segmentation by a thresholding method; (d) The final segmentation by the proposed method; (e)-(f) Manual segmentations.

The running time is about 25 seconds. Quantitative comparisons are given in Table I and Table II. The two tables compare the proposed approach with the methods developed by Staal [15], Mendonça [5], Wang [9], Chen [16], and also with the manual method (Set B). The two tables are incomplete since some values are unavailable in the literatures. The results shows an improvement of our method in sensitivity and accuracy.

TABLE I

COMPARISON OF DIFFERENT SEGMENTATION METHODS (STARE)

STARE	SE	SP	AC
Staal [15]	0.6898±0.1558	0.9793±0.0133	0.9516
Mendonça [5]	0.7123	0.9758	0.9479±0.0123
Wang [9]	0.7543±0.0596	0.9785±0.0106	-
Chen [16]	0.7737±0.0735	0.9738±0.0169	0.9490±0.0109
Ours	0.7208±0.0695	0.9759±0.0076	0.9503±0.0089
Set B	0.8951±0.1085	0.9385±0.0260	0.9350±0.0168

TABLE II

COMPARISON OF DIFFERENT SEGMENTATION METHODS (DRIVE)

DRIVE	SE	SP	AC
Staal [15]	0.7194±0.0694	0.9773±0.0087	0.9441±0.0065
Mendonça [5]	0.7315	0.9781	0.9463±0.0065
Wang [9]	0.7810±0.0340	0.9770±0.0071	-
Chen [16]	0.7589±0.0449	0.9778±0.0064	0.9462±0.0057
Ours	0.7732±0.0345	0.9685±0.0064	0.9445±0.0049
Set B	0.7760±0.0594	0.9725±0.0083	0.9473±0.0048

IV. CONCLUSIONS AND FUTURE WORKS

The paper presents a hybrid method based on Hessian-based multiscale filtering, radial symmetry transform and iterated graph cuts, so as to perform vessel extraction from retinal images. The experimental results demonstrate the efficiency of the proposed method on the two public databases. It can remove boundary effects around the pathological changes, the optic disc by using the radial symmetry transform method. In the future, we plan to improve the efficiency of the iterated graph cuts algorithm. The max-flow/min-cut algorithm proceeds iteratively but it can be parallelized for acceleration.

V. ACKNOWLEDGMENTS

Many thanks to Staal $et\ al.$ and Hoover $et\ al.$ for their STARE and DRIVE databases, and also to the anonymous reviewers for their comments.

REFERENCES

[1] D. Becker, A. Can, J. Turner, H. Tanenbaum, and B. Roysam, "Image processing algorithms for retinal montage synthesis, mapping, and real-time location determination," *Biomedical Engineering, IEEE Transactions on*, vol. 45, no. 1, pp. 105–118, 2002.

[2] L. Zhou, M. Rzeszotarski, L. Singerman, and J. Chokreff, "The detection and quantification of retinopathy using digital angiograms," *Medical Imaging, IEEE Transactions on*, vol. 13, no. 4, pp. 619–626, 2002.

[3] D. Friedman, R. Wolfs, B. O'colmain, B. Klein, H. Taylor, S. West, M. Leske, P. Mitchell, N. Congdon, and J. Kempen, "Prevalence of open-angle glaucoma among adults in the United States." *Archives of ophthalmology*, vol. 122, no. 4, p. 532, 2004.

[4] M. Niemeijer, B. van Ginneken, J. Staal, M. Suttorp-Schulten, and M. Abramoff, "Automatic detection of red lesions in digital color fundus photographs," *Medical Imaging, IEEE Transactions on*, vol. 24, no. 5, pp. 584–592, 2005.

[5] A. Mendonça and A. Campilho, "Segmentation of retinal blood vessels by combining the detection of centerlines and morphological reconstruction," *Medical Imaging, IEEE Transactions on*, vol. 25, no. 9, pp. 1200–1213, 2006.

[6] B. Lam, Y. Gao, and A. Liew, "General Retinal Vessel Segmentation Using Regularization-Based Multiconcavity Modeling," *Medical Imaging, IEEE Transactions on*, vol. 29, no. 7, pp. 1369–1381, 2010.

[7] M. Sofka and C. Stewart, "Retinal vessel centerline extraction using multiscale matched filters, confidence and edge measures," *Medical Imaging, IEEE Transactions on*, vol. 25, no. 12, pp. 1531–1546, 2006.

[8] J. Soares, J. Leandro, R. Cesar, H. Jelinek, and M. Cree, "Retinal vessel segmentation using the 2-D Gabor wavelet and supervised classification," *Medical Imaging, IEEE Transactions on*, vol. 25, no. 9, pp. 1214–1222, 2006.

[9] L. Wang, A. Bhalerao, and R. Wilson, "Analysis of retinal vasculature using a multiresolution hermite model," *Medical Imaging, IEEE Transactions on*, vol. 26, no. 2, pp. 137–152, 2007.

[10] C. Zhou, H. Chan, B. Sahiner, L. Hadjiiski, A. Chughtai, S. Patel, J. Wei, J. Ge, P. Cascade, and E. Kazerooni, "Automatic multiscale enhancement and segmentation of pulmonary vessels in CT pulmonary angiography images for CAD applications," *Medical Physics*, vol. 34, p. 4567, 2007.

[11] G. Loy and A. Zelinsky, "Fast radial symmetry for detecting points of interest," *Pattern Analysis and Machine Intelligence, IEEE Transactions on*, pp. 959–973, 2003.

[12] Y. Li, J. Sun, C. Tang, and H. Shum, "Lazy snapping," *ACM Transactions on Graphics (ToG)*, vol. 23, no. 3, pp. 303–308, 2004.

[13] Y. Boykov and V. Kolmogorov, "An experimental comparison of min-cut/max-flow algorithms for energy minimization in vision," *Pattern Analysis and Machine Intelligence, IEEE Transactions on*, vol. 26, no. 9, pp. 1124–1137, 2004.

[14] A. Hoover, V. Kouznetsova, and M. Goldbaum, "Locating blood vessels in retinal images by piecewise threshold probing of a matched filter response," *Medical Imaging, IEEE Transactions on*, vol. 19, no. 3, pp. 203–210, 2002.

[15] J. Staal, M. Abràmoff, M. Niemeijer, M. Viergever, and B. van Ginneken, "Ridge-based vessel segmentation in color images of the retina," *Medical Imaging, IEEE Transactions on*, vol. 23, no. 4, pp. 501–509, 2004.

[16] J. Chen, J. Tian, Z. Tang, J. Xue, Y. Dai, and J. Zheng, "Retinal vessel enhancement and extraction based on directional field," *Journal of X-Ray Science and Technology*, vol. 16, no. 3, pp. 189–201, 2008.